Part I
Preparation and Characterization of Carbon Nanotubes

Carbon Nanotube and Related Field Emitters: Fundamentals and Applications. Edited by Yahachi Saito

ISBN: 978-3-527-32734-8

1
Structures and Synthesis of Carbon Nanotubes

Yahachi Saito

1.1
Structures of Carbon Nanotubes

Carbon nanotubes (CNTs) are hollow cylinders made of seamlessly rolled graphene (honeycomb lattice of carbon atoms, Figure 1.1) with diameters ranging from about 1 over 50 nm, depending on the number of walls comprising the nanotubes. Structurally well-ordered CNTs were discovered and their structures were well characterized by Iijima in 1991 [1]. CNTs composed of one sheet of graphene are called *single-wall carbon nanotube*s (abbreviated SWCNTs or SWNTs) [2–4], and those made of more than two sheets, multiwall carbon nanotubes (abbreviated MWCNTs or MWNTs). The length of nanotubes exceeds 10 μm, and the longest ones are reportedly on the order of a centimeter [5, 6].

1.1.1
Single-Wall CNTs

There are numerous ways of rolling a sheet of the honeycomb pattern into a seamless cylinder, which give rise to a vast range of diameters and various helical structures. The structure of a CNT is specified (except for handedness) by a vector connecting two lattice points in an unrolled honeycomb lattice (e.g., points O and A in Figure 1.1). When the honeycomb sheet is rolled so as to make the two points coincide, a cylinder whose circumference corresponding to the line AO is formed. Such a vector connecting the crystallographically equivalent lattice points in an unrolled lattice and being perpendicular to the tube axis is called the *chiral vector* (or wrapping vector), which is expressed using two fundamental translational vectors $\boldsymbol{a}_1$, $\boldsymbol{a}_2$:

$$\boldsymbol{C}_\mathrm{h} = n\boldsymbol{a}_1 + m\boldsymbol{a}_2 \equiv (n, m) \tag{1.1}$$

where n and m are integers with $0 \leq |m| \leq n$. The sets of two integers (n, m) are called *chiral indices*, which are used to specify the structure of SWNTs. The diameter

Carbon Nanotube and Related Field Emitters: Fundamentals and Applications. Edited by Yahachi Saito

ISBN: 978-3-527-32734-8

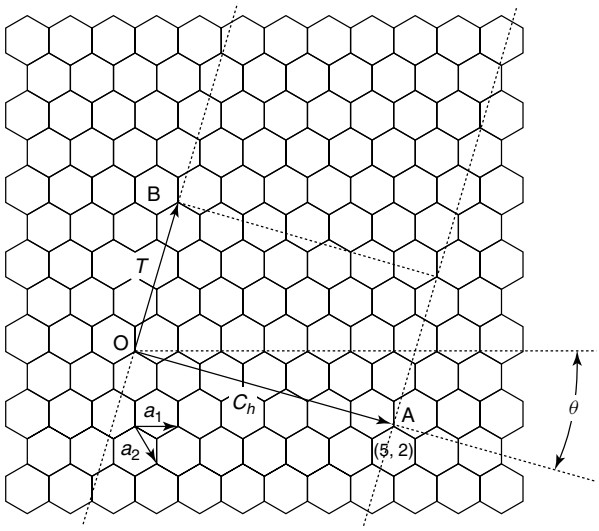

Figure 1.1 Graphene (a sheet of honeycomb lattice of carbon atoms). A carbon nanotube is a seamless cylinder made of a rolled graphene by superimposing the two lattice points, for example, O and A. $\boldsymbol{C}_h$ and $\boldsymbol{T}$ for chiral indices (5, 2) are illustrated.

d_t and chiral angle θ (Figure 1.1) can be expressed in terms of n and m

$$d_t = a\sqrt{n^2 + nm + m^2}\Big/\pi \tag{1.2}$$

$$\theta = \cos^{-1}\left(\frac{2n+m}{2\sqrt{n^2+nm+m^2}}\right) \quad (|\theta| \le \pi/6) \tag{1.3}$$

where $a = |\boldsymbol{a}_1| = |\boldsymbol{a}_2| = 0.246\,\text{nm}$.

A SWNT has translational symmetry along the tube axis. The basic translational vector T is represented by

$$T = \left\{(2m+n)\boldsymbol{a}_1 - (2n+m)\,\boldsymbol{a}_2\right\}\Big/ d_R \tag{1.4}$$

where d_R is defined by using the greatest common divisor D_G of n and m as follows:

$$d_R = \begin{cases} D_G & \text{if } n-m \text{ is not a multiplie of } 3D_G \\ 3D_G & \text{if } n-m \text{ is a multiplie of } 3D_G \end{cases} \tag{1.5}$$

CNTs with $n = m(\theta = \pi/6)$ and $m = 0\,(\theta = 0)$, called *armchair* type and *zigzag* type, respectively, do not have helicity. CNTs with other chiral indices ($n \neq m \neq 0$) have helical structures and are called *chiral type*. In Figure 1.2a–c, structure models of armchair, zigzag, and chiral type CNTs, respectively, are shown.

The diameter of SWNTs actually synthesized ranges from 0.7 to about 3 nm, depending on synthesis conditions especially on the diameter of catalyst particles employed for the synthesis. Figure 1.3 shows a transmission electron microscope (TEM) image of SWNTs, with diameter ranging between 1.0 and 1.3 nm, produced

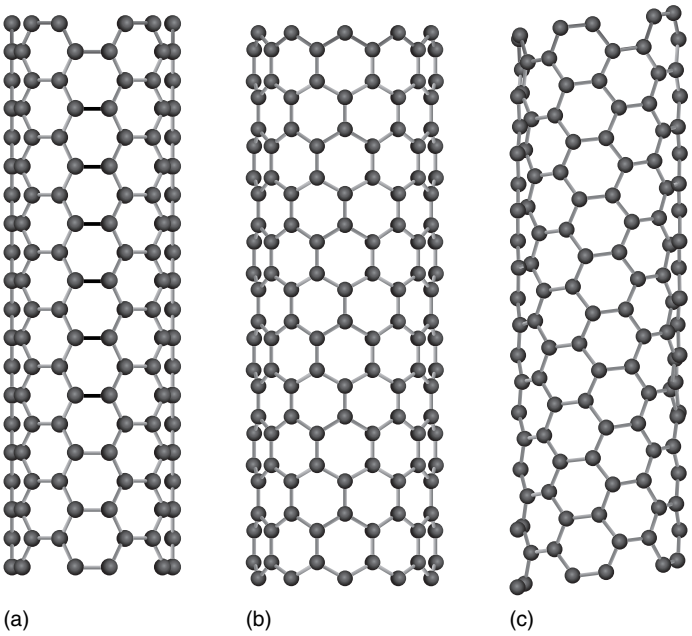

Figure 1.2 Structure models CNTs: (a) (5, 5) armchair, (b) (10, 0) zigzag, and (c) (4, 6) chiral type.

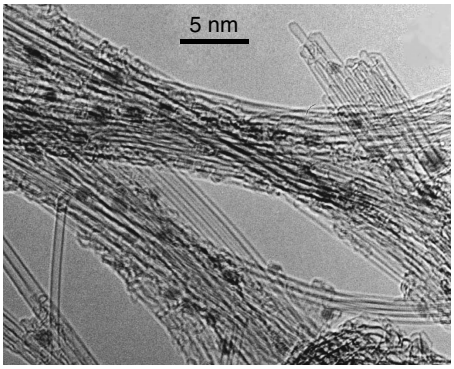

Figure 1.3 TEM picture of SWNTs produced by arc discharge with Ni catalyst.

by arc discharge with a Ni catalyst. The ends of a tube made from a rolled graphene remain open, but CNTs actually synthesized are capped by a curved graphene (Figure 1.3) or by a metal particle used as catalyst in the synthesis process. Pentagons (five-membered rings) have to be inserted into a graphene sheet in order to render a positive curvature to the sheet. Since one pentagon introduces a $+\pi/6$ wedge disclination in the honeycomb lattice, six pentagons are required to from a hemispherical dome of a curved graphene, like the half of the C_{60} fullerene, and to close one end of a CNT. The caps of CNTs with small diameters (less than about 4 nm in diameter) such as SWNTs look spherical (see the ends of SWNTs

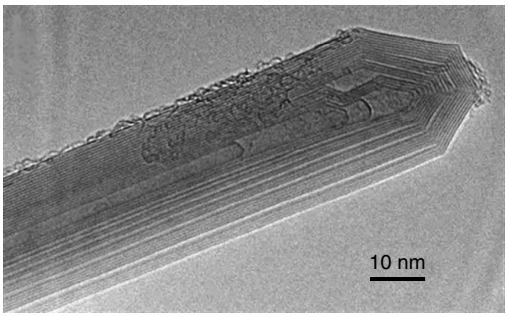

Figure 1.4 TEM picture of MWNTs produced by arc discharge.

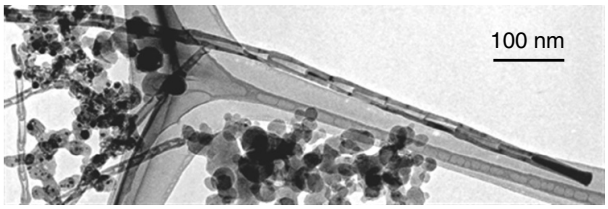

Figure 1.5 TEM picture of a bamboo-shaped MWNT.

in Figure 1.3), while those of thick CNTs (e.g., MWNTs) exhibit polyhedral shapes because the pentagon sites extrude like corners of the polyhedra (see Figure 1.4 in the next section).

1.1.2 Multiwall CNTs

An ideal MWNT consists of graphene sheets stacked in a concentric way. MWNTs produced by the arc-discharge technique (see below) have a high structural perfection and are straight, as shown in Figure 1.4. The number of sheets ranges from 2 to about 40. For thick MWNTs composed of more than three or four layers, the interlayer spacing between rolled graphene sheets is 0.344 nm on average [7]. The spacing is wider by a small percentage than the ideal graphite value (0.3354 nm), being characteristic of the turbostratic carbon (graphitic layers that are stacked in parallel but without translational and rotational relations between the adjacent layers) [8]. The diameters of MWNTs are in the range 4–50 nm, and the lengths are over 10 μm. MWNTs contain narrow cavities (approximately 2–10 nm in diameter) in the center.

On the other hand, MWNTs synthesized by thermal decomposition of hydrocarbon gases (so-called chemical vapor deposition (CVD), see below) are in general comprised of defective graphene sheets and are sometimes curved and curled. Bamboo-like structures composed of a series of compartments with a metal catalyst at their tips are formed as shown in Figure 1.5 [9]. The graphite layers in a bamboo-structured MWNT are not parallel to the tube axis but are inclined to form stacked cones.

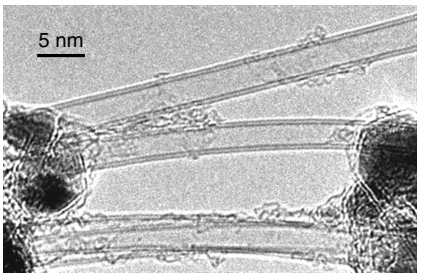

Figure 1.6 TEM image of DWCNTs produced by arc discharge.

1.1.3
Thin-Walled CNTs

Double-wall carbon nanotubes (DWNTs or DWCNTs) consisting of two layers of graphene can be selectively prepared by arc discharge and CVD. Figure 1.6 shows a typical TEM image of DWCNTs produced by arc discharge in a He/H_2 gas mixture with Fe–Co–Ni as catalyst and sulfur as promoter [10]. The diameter of DWCNTs is in the range 3–4 nm, that is, intermediate between those of SWNTs and thick MWNTs. The interlayer spacing between the outer and inner walls ranges from 0.37 to 0.39 nm, being about 10% wider than that of thick MWNTs. Due to the small diameter of DWCNTs, the electric voltage required for field emission from DWCNTs is as low as that for SWNTs, though DWCNTs are more robust against degradation during field emission than SWNTs because of the smaller curvature (i.e., more stable with the smaller strains) and the larger cross section (two layers) for electron flow.

1.2
Synthesis of Carbon Nanotubes

Production methods of CNTs are roughly divided into three categories: (i) electric arc discharge between carbon electrodes, (ii) laser vaporization of a carbon target, and (iii) thermal decomposition of hydrocarbon gases or CVD. The arc discharge and CVD techniques are briefly described here. Concerning the laser ablation method, which is mainly used for the preparation of high-purity SWNTs, the details can be found in [11].

1.2.1
Arc Discharge

A direct current (DC) arc is almost exclusively used because it is amenable and provides a high yield of nanotubes, even though an alternating current (AC) arc can also evaporate carbon electrodes. Both the anode and the cathode are made of graphite rods for producing MWNTs, while a metal (or metal oxide) powder is impregnated into the anode for the production of SWNTs. The metal catalyzes the formation of SWNTs. Typical catalysts are Fe–Ni, Co–Ni, Y–Ni, and Rh–Pt [12].

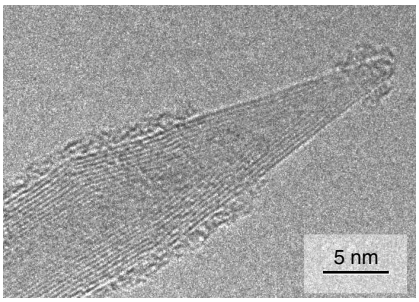

Figure 1.7 TEM picture of a MWNT with a cone-shaped tip. The cone angle is 19.2°, indicating the presence of five pentagons at the apex.

Carbon electrodes are evaporated in a buffer gas (usually helium) at a desired pressure (200–600 Torr for helium gas). Since the anode surface is heated to a higher temperature (~4000 K) than the cathode surface (~3500 K), the anode is selectively consumed in the arc. The position of the anode tip must be adjusted in order to maintain the proper spacing (about 1 mm) between the electrodes. Approximately half of the evaporated carbon condenses on the tip of the cathode, forming a cylindrical hard deposit. MWNTs are obtained inside the cylindrical cathode deposit even without metal catalysts. The remaining carbon vapor condenses in a gas phase, forming soot. Fullerenes such as C_{60} and C_{70} are grown in the soot. When the catalyst metal is co-evaporated with carbon, SWNTs are formed and found in the soot deposited on the walls of the reaction chamber and on the surface of the cathode.

For the production of MWNTs, pure carbon is evaporated mainly in helium gas. Hydrogen gas and even air can also be employed as the working gas. In the latter case, relatively ''clean'' MWNTs are produced (i.e., the amount of byproducts such as carbon nanoparticles is very small [13]).

Radio frequency (RF) plasma heating of graphite in argon gas can be used to synthesize MWNTs, which are characterized by their cone-shaped tip [14]. The cone angle is 19.2°, indicating the presence of five pentagons at the apex (Figure 1.7). The outer diameter of the cylinder part is approximately 10 nm.

1.2.2 Chemical Vapor Deposition

Thermal or plasma-assisted decomposition of gaseous carbon molecules can be used to produce a variety of CNTs ranging from SWNTs to MWNTs. The commonly used carbon sources are methane, acetylene, alcohol, and carbon monoxide. The decomposition of molecules is assisted on the surface of small catalytic particles, and it is believed that CNTs nucleate and grow using the catalyst as a scaffold. The most effective catalysts are Fe, Ni, and Co. This technique enables the formation of CNTs directly on solid substrates on which metal catalyst are deposited, and is therefore called *catalytic chemical vapor deposition*. CVD is the term used to describe heterogeneous reactions in which both solid and gaseous products are formed

from a gaseous precursor through chemical reaction. CVD methods have several advantages over the other methods such as arc discharge: CNTs can be grown on various solid substrates, and a wide range of process parameters makes the control over the morphology and structure of the products easy. Moreover, since the CVD method is compatible with the present-day microfabrication technique for Si-based integrated circuits, catalytic CVD is now attracting considerable attention for the fabrication of CNT-based nanoelectronic devices as well as emitter arrays in field-emission displays.

In this subsection we focus on a growth method on a substrate by which CNTs are formed in a controlled position (patterned area) on a solid surface and also aligned vertically to the substrate. Concerning vapor-phase growth or the floating catalyst methods in which both carbon-bearing gases and catalysts are injected into a reaction chamber without a substrate, the reader can consult reviews on the subject [15].

1.2.2.1 **Thermal CVD**

The apparatus for CNT growth by thermal CVD ranges from a simple homemade reactor to automated large ones for industrial production. The simple apparatus consists of a quartz tube (20–50 mm in diameter and about 700 mm in length) inserted into a tubular electric furnace capable of maintaining a high temperature (up to about 1000 °C) over a length about 20 cm. This type of system is a hot-wall reactor, inside which solid substrates, typically about 10 square millimeters or larger, are placed and the carbon feedstock gas is supplied with or without dilution through mass flow controllers. Catalyst particles have to be deposited on the substrates. Physical vapor deposition techniques (sputtering and vacuum evaporation) as well as wet chemistry can be used to prepare catalysts including transition metals onto the substrates. The temperature for the synthesis of CNTs by CVD is generally in the range 650–900 °C.

Cold-wall reactors, where the substrate is heated by resistive, inductive, or infrared (IR) radiation heaters, can also be employed for low-pressure operations. It is reported that the employment of a hot filament enables MWNTs to grow at the substrate temperature of 400 °C [16].

CNTs synthesized by CVD generally contain metal particles as residue of the catalyst on their tips or roots. Formation of CNTs aligned vertically to the substrate surface is another characteristic of the CVD technique. This alignment occurs when CNTs grow densely on the surface because the adjacent CNTs support each other from falling down.

1.2.2.2 **Plasma-Enhanced CVD**

The plasma-enhanced chemical vapor deposition (PECVD) method involves a glow discharge in a reaction chamber through a high-frequency voltage applied to the electrodes. PECVD was first introduced in the fabrication of microelectronic devices in order to enable the CVD process to proceed at reduced temperatures of a substrate because the substrate cannot tolerate the elevated temperature of some thermal CVD processes. The common PECVD processes proceed at substantially

lower substrate temperatures (room temperature to 100 °C). Low-temperature operation is possible because the dissociation of the precursor for the deposition of semiconductor, metal, and insulating films is enabled by the high-energy electrons in a cold plasma.

In CNT growth by CVD, on the other hand, dissociation of the precursor (carbon-containing molecules) on the surface of catalytic particles is the critical process, and therefore precursor dissociation in the gas phase is not necessary though some activation or excitation of molecules may contribute to the reduction of the substrate temperature. When precursor dissociation occurs in the gas phase, an excessive amount of amorphous carbon is produced. There may be a minimum temperature to which the substrate has to be heated because precursor dissociation on the catalyst surface is the key to CNT growth. MWNTs are reportedly grown at 430 and 500 °C by PECVD [17, 18]. CNTs grown by PECVD contain more defects in their structures than those grown by arc discharge and thermal CVD because of damages by ion bombardment.

1.3 Electrical and Mechanical Properties of Carbon Nanotubes

1.3.1 Electronic Structure

CNTs are predicted to be metallic or semiconductive depending on their chiral indices (n, m). When $n - m = 3j$, where j is an integer, the tube is metallic. Strictly, the effect of tube curvature is to open a very tiny gap (on the order of millielectron volts) at the Fermi level for metallic tubes with $n - m = 3j$, while armchair-type tubes ($n = m$) are always metallic because they are independent of curvature. All other tubes (i.e., $n - m \neq 3j$) are true semiconductors. A slight change in the wrapping angle of a hexagonal lattice drastically changes their conductive properties. The energy gap of semiconducting CNTs is approximately inversely proportional to the tube diameter, and to be independent of the chiral angle (wrapping angle), according to the tight binding calculation, the energy gap E_g is given by

$$E_g = 2\gamma a_{C-C}/d_t \tag{1.6}$$

where γ is the nearest neighbor interaction energy, $a_{C-C} = 0.142$ nm being the carbon–carbon bond distance, and d_t is the nanotube diameter [19]. The $1/d_t$ dependence is really observed experimentally for SWNTs with diameters between 1 and 2 nm. The reported values of the tight binding parameter γ are in the range 2.4–2.9 eV [20].

The electronic structures of SWNTs have been extensively studied by resonance Raman scattering spectroscopy [21], photo-absorption and luminescence spectroscopy [22], scanning tunneling microscopy (STM) [23, 24], and so on. The electronic density of states (DOS) of SWNTs are characterized by the presence of

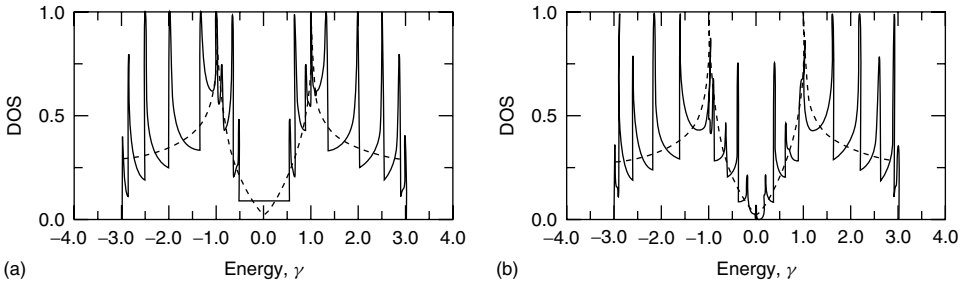

Figure 1.8 The electronic density of states (DOS) of (a) a metallic (9, 0) and (b) a semiconducting (10, 0) SWNT. Spikelike peaks called *van Hove singularities* are characteristic of one-dimensional material. Broken lines represent the DOS of a graphene sheet. (Reprinted with permission from Saito, R. *et al*. (1992) *Appl. Phys. Lett*., **60**, 2204. Copyright 1992, American Institute of Physics.)

a series of spikelike peaks called *van Hove singularities* as shown in Figure 1.8, reflecting one-dimensional (1D) materials [25].

1.3.2 Electric Properties

CNTs exhibit quantum mechanical electric transport phenomena owing to their small size and structural perfection, and the ballistic transport of electrons over 1 μm distance is also expected because the backscattering of conduction electrons by lattice defects (such as impurity ions) with long-range potentials is annihilated in CNTs [26]. Metallic CNTs can act as tiny wires, and semiconducting ones can be envisioned to act as transistors. The two-terminal conductance of a metallic CNT is given by Landauer formula for 1D conductors [27]:

$$G = \left(2e^2/h\right) \cdot \sum_{i}^{N} T_i \tag{1.7}$$

where $2e^2/h = G_0 \approx 1/\left(12.9\,\mathrm{k\Omega}\right)$ is the quantum unit of conductance, and T_i is the transmission of the ith conducting channel. When $T_i = 1$, corresponding to the case of no scattering inside the CNT and at the contacts to electrodes, a metallic SWNT is expected to have a resistance $R = 1/2G_0 \approx 6.5\,\mathrm{k\Omega}$, because there are two channels of conductance near the Fermi level [26].

In the case of scattering within a CNT, an effective mean free path is used to describe the scattering probability of conduction electrons. Elastic scattering caused by a potential irregularity such as impurity ions and inelastic scattering by phonons contribute to the effective mean free path λ_{eff}:

$$\frac{1}{\lambda_{\mathrm{eff}}} = \frac{1}{\lambda_{\mathrm{el}}} + \frac{1}{\lambda_{\mathrm{ac}}} + \frac{1}{\lambda_{\mathrm{op}}} \tag{1.8}$$

where λ_{el} is the mean free path for elastic scattering and λ_{ac} and λ_{op} are the mean free paths for scattering by acoustic and optical phonons, respectively. Due

to the backscattering constraint, the elastic scattering is drastically reduced to $\lambda_{el} \geq 1\,\mu m$. Acoustic phones contribute weakly to inelastic scattering as well, with $\lambda_{ac} \approx 1\,\mu m$ [28]. Thus, conduction electrons in metallic CNTs at low energies (under low electric field) transport without scattering (i.e., ballistic) for a long distance of 1 μm or so. On the other hand, optical phone can scatter efficiently once the energy of conduction electrons exceed optical phonon energies (~180 meV), with $\lambda_{op} \approx 20-30\,nm$ [29, 30]. This results in current saturation at elevated biases and can lead to Joule heating and breakdown of CNTs. For semiconducting CNTs, there are indications that at low energies λ_{eff} is on the order of a few hundred nanometers [29, 30].

The low scattering probability together with strong chemical bonding and high thermal conductivity of CNTs allows them to withstand extremely high current densities up to $\sim 10^9$ A cm^{-2} [31].

1.3.3 Mechanical Properties

Since the basal-plane elastic modulus of graphite is larger than that of any other known materials, CNTs that are formed by seamlessly rolling graphitic sheets are predicted to be extraordinary stiff and strong. Theoretical estimates predict that CNTs have a Young's modulus of the order of 1 TPa [32–34]. Their high stiffness, coupled with their low density, implies that the nanotube might be useful as nanoscale mechanical parts. Young's moduli of isolated MWNTs were measured to be in a range from ~0.1 to ~2 TPa by various methods [35–37], which include observations of thermal vibration and resonance vibration in TEM and stress–strain measurements by an atomic force microscope (AFM). The variation of the measured moduli is considered to be due the difference in the CNT structure (e.g., layer numbers and presence/absence of the bamboo structure), length of a CNT cantilever, and error of temperature measurement. The moduli at lower bound are possibly caused by the occurrence of kinks on the compressed side (inner arc) of a bent CNT. Since the kinks are liable to occur at a smaller bent for a larger diameter CNT, the moduli show a decreasing trend with the increase of diameter [37].

Tensile strength of arc-grown MWNTs has been measured to be in a range 11–63 GPa by a tension test in TEM [36] and 150 ± 45 GPa by AFM [39]. For SWNTs, a high value of tensile strength, about 200 GPa, has been reported [38]. However, a bundle of CVD-grown MWNTs is reported to give much lower strength, 1.72 GPa [39], which is due to structural defects and sliding between adjacent MWNTs.

The most distinguished mechanical property of nanotubes is their unusual strength in the large-strain region. CNTs can be bent repeatedly through large angles (up to ~110°) without undergoing catastrophic fracture, despite the occurrence of kinks [40], being remarkably flexible and resilient.

1.3.4
Heat-Transport Properties

Carbon materials such as diamond and graphite have the highest thermal conductivity near room temperature among materials because of the strong carbon–carbon chemical bonds and light mass of carbon atoms. Phonons (lattice vibrations) are the major and exclusive carriers of heat for graphite and diamond, respectively. Thermal conductivity of a test piece strongly depends on the grain sizes in the specimen. Therefore, the high crystallinity and directionality of CNTs promise their thermal conductivity to be equal to or higher than those of graphite parallel to the basal planes (maximum of $\sim$3000 W$(m\cdot K)^{-1}$ at 100 K, $\sim$2000 W$(m\cdot K)^{-1}$ at 300 K) [41] and natural diamond (maximum $\sim 10^4$ W $(m\cdot K)^{-1}$ at 80 K, $\sim$2000 W $(m\cdot K)^{-1}$ at 300 K) [42].

Thermal conductivities of an isolated MWNT with diameter of 14 nm and bundles of MWNTs (bundle diameters of 80 and 200 nm) have been measured using a microfabricated suspended device in the temperature range 8–370 K [43]. The isolated, suspended MWNTs exhibit thermal conductivity of more than 3000 W $(m\cdot K)^{-1}$ at room temperature, which is 1–2 orders of magnitude higher than those for aligned bundles or macroscopic mat samples. Anisotropic thermal conductivities in aligned SWNT films have been observed [44]: 40–60 W $(m\cdot K)^{-1}$ along the fiber direction and about 11 W $(m\cdot K)^{-1}$ perpendicular to the fiber direction.

References

1. Iijima, S. (1991) *Nature*, **354**, 56.
2. Iijima, S. and Ichihashi, T. (1993) *Nature*, **363**, 603.
3. Bethune, D.S., Kiang, C.H., de Vries, M.S., Gorman, G., Savoy, R., Vazquez, J., and Beyers, R. (1993) *Nature*, **363**, 605.
4. Saito, Y., Yoshikawa, T., Okuda, M., Fujimoto, N., Sumiyama, K., Suzuki, K., Kasuya, A., and Nishina, Y. (1993) *J. Phys. Chem. Solids*, **54**, 1849.
5. Zheng, L.X., O'Connel, M.J., Doorn, S.K., Liao, X.Z., Zhao, Y.H., Akhadov, E.A., Hoffbauer, M.A., Roop, B.J., Jia, Q.X., Dye, R.C., Peterson, D.E., Huang, S.W., and Liu, J. (2004) *Nat. Mater.*, **3**, 673.
6. Yun, Y., Shanov, V., Tu, Y., Subramaniam, S., and Schulz, M.J. (2006) *J. Phys. Chem. B*, **110**, 23920.
7. Saito, Y., Yoshikawa, T., Bandow, S., Tomita, M., and Hayashi, T. (1993) *Phys. Rev. B*, **48**, 1907.
8. See for example Kelly, B.T. (1981) *Physics of Graphite*, Chapter 1, Applied Science Publishers, London.
9. Saito, Y. and Yoshikawa, T. (1993) *J. Cryst. Growth*, **134**, 154.
10. Saito, Y., Nakahira, T., and Uemura, S. (2003) *J. Phys. Chem. B*, **107**, 931.
11. Thess, A., Lee, R., Nikolaev, P., Dai, H., Petit, P., Robert, J., Xu, C., Lee, Y.H., Kim, S.G., Rinzler, A.G., Colbert, D.T., Scuseria, G.E., Tomanek, D., Fischer, J.E., and Smalley, R.E. (1996) *Science*, **273**, 483.
12. Saito, Y. (1999) *New Diamond Front. Carbon Technol.*, **9**, 1.
13. JFE Engineering Corporation (2004) JEF Technical Report No. 3, March 2004, CNT Tape of High Purity, p. 78 (in Japanese).
14. Koshio, A., Yudasaka, M., and Iijima, S. (2002) *Chem. Phys. Lett.*, **356**, 595.
15. See for example Govindaraj, A. and Rao, C.N.R. (2006) *Carbon*

Nanotechnol, Chapter 2 (ed. L.Dai), Elsevier, Amsterdam.
16. (a) Nihei, M., Kawabata, A., Hyakushima, T., Sato, S., Nozue, T., Kondo, D., Shioya, H., Iwai, T., Ohfuchi, M., and Awano, Y. (2006) Proceedings of the International Conference on Solid State Devices and Materials, p. 140; (b) Ishikawa, Y. and Ishizuka, K. (2009) *Appl. Phys. Express*, **2**, 045001.
17. Sakuma, N., Katagiri, M., Sakai, T., Suzuki, M., Sato, S., Nihei, M., Nihei, Awano, Y., and Kawarada, H. (2007) New Diamond and Nano Carbon, Abstract Book, p. 195.
18. Honda, S., Katayama, M., Lee, K.-Y., Ikuno, T., Ohkura, S., Oura, K., Furuta, H., and Hirao, T. (2003) *Jpn. J. Appl. Phys.*, **42**, L441.
19. White, C.T. and Mintmire, J.W. (1998) *Nature*, **394**, 29.
20. Odom, T.W., Huang, J.-L., Kim, P., and Lieber, C.M. (1998) *Nature*, **391**, 62.
21. Saito, R. and Kataura, H. (2001) *Carbon Nanotubes; Synthesis, Structure, Properties, and Applications* (ed. M. S. Dresselhaus *et al.*), Springer, Berlin, pp. 213–246.
22. O'Connell, M., Bachilo, S.M., Huffman, C.B., Moore, V., Strano, M.S., Haroz, E., Rialon, K., Boul, P.J., Noon, W.H., Kittrell, C., Ma, J., hauge, R.H., Weisman, R.B., and Smalley, R.E. (2002) *Science*, **297**, 593.
23. Tan, S.J., Devoret, M.H., Dai, H., Thess, A., Smalley, R.E., Greerligs, L.J., and Dekker, C. (1997) *Nature*, **386**, 474.
24. Wildoer, J.W.G., Venema, L.C., Rinzler, A.G., Smalley, R.E., and Dekker, C. (1998) *Nature*, **391**, 59.
25. Saito, R., Fujita, M., Dresselhaus, G., and Dresselhaus, M.S. (1992) *Appl. Phys. Lett.*, **60**, 2204.
26. Ando, T. (2005) *J. Phys. Soc. Jpn.*, **74**, 777.
27. Landauer, R. (1970) *Philos. Mag.*, **21**, 863.
28. Avouris, P. (2004) *MRS Bull.*, **29**, 403.
29. Wind, S.J., Appenzeller, J., and Avouris, P. (2003) *Phys. Rev. Lett.*, **91**, 058301.
30. Yaish, Y., Park, J.Y., Rosenblatt, S., Sazonova, V., Brink, M., and McEuen, P.L. (2004) *Phys. Rev. Lett.*, **92**, 046401.
31. Wang, Z.L., Gao, R.P., de Heer, W.A., and Poncharal, P. (2002) *Appl. Phys. Lett.*, **80**, 856.
32. Lu, J.P. (1997) *Phys. Rev. Lett.*, **79**, 1297.
33. Zhang, P., Huang, Y., Geubelle, P.H., Klein, P.A., and Hwang, K.C. (2002) *Int. J. Solids Struct.*, **39**, 3893.
34. Li, C. and Chou, T.W. (2003) *Compos. Sci. Technol.*, **63**, 1517.
35. Treacy, M.M.J., Ebbesen, T.W., and Gibson, J.M. (1996) *Nature*, **381**, 678.
36. Yu, M.F., Lourie, O., Dyer, M.J., Moloni, K., Kelly, T.F., and Ruoff, R.S. (2000) *Science*, **287**, 637.
37. Poncharal, P., Wang, Z.L., Ugarte, D., and de Heer, W.A. (1999) *Science*, **283**, 1513.
38. Kong, J., Soh, H.T., Cassell, A.M., Quante, C.F., and Dai, H. (1998) *Nature*, **395**, 878.
39. Pan, Z.W., Xie, S.S., Lu, L., Chang, B.H., Sun, L.F., Zhou, W.Y., Wang, G., and Zhang, D.L. (1999) *Appl. Phys. Lett.*, **74**, 3152.
40. Iijima, S., Brabec, C., Maiti, A., and Bernholc, J. (1996) *J. Chem. Phys.*, **104**, 2089.
41. Kelly, B.T. (1981) *Physics of Graphite*, Chapter 4, Applied Science Publisher, London.
42. Barman, S. and Srivastava, G.P. (2007) *J. Appl. Phys.*, **101**, 123507.
43. Kim, P., Shi, L., Majumdar, A., and McEuen, P.L. (2001) *Phys. Rev. Lett.*, **87**, 215502.
44. Fischer, J.E., Zhou, W., Vavro, J., Llaguno, M.C., Guthy, C., Haggenmueller, R., Casavant, M.J., Walters, D.E., and Smalley, R.E. (2003) *J. Appl. Phys.*, **93**, 2157.